Recovery of nickel from strongly acidic bio-ore leachate using a bispicolylamine-based chelating resin

Bastien Jally, Mathilde François, Morgane Kessler, Baptiste Laubie, Marie-Odile Simonnot

Recovery of nickel from strongly acidic bio-ore leachate using a bispicolylamine-based chelating resin

Bastien Jally, Mathilde François, Morgane Kessler, Baptiste Laubie, Marie-Odile Simonnot*

Université de Lorraine, CNRS, LRGP, F-54000 Nancy, France

ABSTRACT

Given the increasing demand for nickel (Ni) in the Li-ion battery industry, the agromining chain of processes, based on phytomining of Ni combined with hydrometallurgy, has the potential to form an important source of Ni. Currently, plants grown on Ni-rich soils (in this case *Odontarrhena chalcidica*), having hyperaccumulated Ni, are ashed, and the Ni is transferred from ash to solution by sulfuric acid leaching. This work focuses on the recovery of Ni-sulfate from this strongly acidic leachate that contains many cations. For this purpose, a bispicolylamine-based chelating resin (Dowex M4195) was tested to better understand the functioning of this resin under these conditions.

Column experiments were performed with model synthetic solutions containing Ni and Na-sulfate at pH 2. A set of reactions has been formulated to describe the interactions involved and used in a model combining transport in porous media and chemical reactions at equilibrium. Excellent agreement between the experimental and the calculated breakthrough curves were obtained by adjusting only two parameters. The set of reactions and parameters allowed to fit with sufficient accuracy the breakthrough curves obtained from an ash leachate of the hyperaccumulator plant *O. chalcidica*.

A better understanding of the use of the Dowex M4195 resin for the extraction of Ni from a strong acid multicomponent solution has been achieved, and this separation has been shown to be promising for the recovery of Ni extracted from hyperaccumulator plant bio-ores as part of the agromining process.

Keywords

Chelating resin; hydrometallurgy; nickel recovery; column experiments; phytomining; agromining

Highlights

- Nickel can be separated from a strong acid solution by a chelate resin.
- Nickel separation was tested by column experiments and modeling.
- A reaction scheme and equilibrium constants model the functioning of Dowex M4195 resin.
- $NiSO_4$ purities of two plant ash leachates were upgraded to 97% and 99%.
- Nickel separation by Dowex M4195 resin is promising for use in the agromining chain.

1. Introduction

The demand for metals is booming, especially because of the decarbonization and the development of electric vehicles using Ni-containing Li-ion batteries. This is reflected in an increase in the price of Ni, which has doubled since 2017 [1]. For this reason, and as mining becomes increasingly challenging with declining ore grades, processes are being developed to exploit secondary resources of Ni which contribute to implementing the circular economy. Among the processes for secondary resources, agromining (also called "phytomining") is attracting substantial interest. The agromining process consists of extracting metals from low concentrations in soils using hyperaccumulator plants by means of phytoextraction [2]. The metals are then recovered by hydrometallurgical processes from the harvested bio-ore. This chain has been developed for Ni due to the interest in this metal and because nearly 3% of the Earth's surface is covered by ultramafic (Ni-rich) soils and more than 500 species of Ni hyperaccumulator plant species have been discovered to date. Recent field studies have evaluated the production of phytomined Ni in several regions of the world (Malaysia, Mexico, Austria) with surfaces from 500 m^2 to 1 ha [3–5]. Nickel agromining is now a staple Nature-Based Solution and using *Odontarrhena chalcidica* annual yields up to 150 kg_{Ni}/ha have been obtained with optimized agronomic practices [6,7].

To recover the Ni present in the plant tissues, several processing routes have been explored. The most advanced and promising processes stem from the recovery of Ni from plant ash, which can contain up to 20% by weight of Ni [8]. Leaching the ash with sulfuric acid at mild temperatures (*ca.* 90 °C) yields a Ni-rich solution containing up to 30 g_{Ni}/L [9], but also unwanted elements, including calcium (Ca), magnesium (Mg), iron (Fe), and potassium (K). Nickel can be separated by solvent extraction [10] or preferential precipitation to obtain Ni-salts or oxides of high purity [8,9,11]. It is essential to implement efficient separation in the hydrometallurgical processing of Ni bio-ores.

To reduce the consumption of reagents, an alternative process can involve ion exchange (IX) and/or selective adsorption using a selective resin composed of polymers beads with functional groups that bind the target metal. The performance and robustness of these resins have been proven by the metallurgical industry in the high-pressure acid leaching process of Ni laterites [12], or for the removal of Ni from cobalt (Co) electrolytic solutions [13]. To exhaust complex multi-metallic solutions from Ni, high selectivity is crucial. To meet this objective, resins with highly selective

functional groups have been developed, and these are called chelating resins. Their functional groups form strong and selective bonds with the target metals. Because they are weak bases or acids, the sorption is reversible, and elution can be conducted by displacing the bound metal with the proton (H^+). Conversely, their main drawback is their limited capacity to treat acidic feeds where H^+ competes with the metal cation. Recently, IX separation processes using chelating resin have gained increasing attention, to concentrate and purify feeds prior to solvent extraction [14], or to treat concentrated Ni feeds originating from lithium ion battery recycling [15], or multimetallic industrial effluent [16].

Bis-2-picolylamine (*bpa*) grafted resin (Fig. 1), marketed as Dowex M4195 (Dow) or Lewatit 220 (Lanxess), is renowned for its high affinity for copper (Cu) and, to a lesser extent, for Ni. Sirola described an analogous silicon polymer grafted with *bpa* (CuWRAM®) for the removal of Ni and Cu from a concentrated solution of zinc sulfate ($ZnSO_4$) [17].

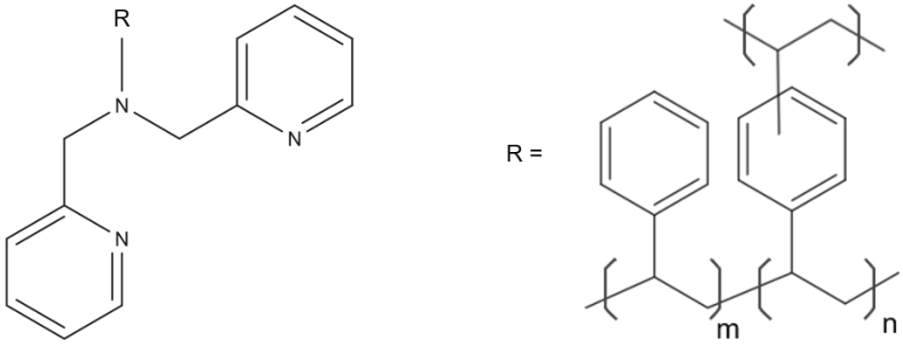

Fig. 1. Structural representation of the *bpa* group grafted on the polymeric matrix (R): polystyrene cross-linked with divinyl-benzene (PS-DVB)

The three nitrogen (N) atoms of the *bpa* group are electron donors and form strong bonds with the transition metals [18]. Thus, the order of selectivity in sulfate media is: Cu(II) >> UO_2(IV) > Ni(II) > Fe(III) > Zn(II) > Co(II) > Cd(II) > Fe(II) [19,20]. In this list, only the retention of uranate anion (UO_2) results from an anion exchange mechanism rather than chelation [21]. The electronic doublets of the N atoms are stabilized by a large π-system, allowing chelation even in acidic media, outperforming conventional weak base groups. The three N atoms can be protonated, but it is difficult

78 to distinguish their behavior and the experimental determination of their dissociation constants K_{ai} ($1 \leq i \leq 3$) is
79 complicated. The first two acidities are far from neutrality [20,22], the inflection points of the titration curves are
80 hardly discernible, and there is no consensus on the pK_{ai} values, which also appears to depend on the acid used.
81 Regarding the third acidity, Grinstead initially suggested that the pK_{a3} value (corresponding to tertiary amine
82 protonation) was 3.5 in sulfate media [20]. Further proton uptake did not yield any inflexion points in the titration
83 curve. Diniz and coworkers reinterpreted the data of Grinstead in sulfate media and proposed 1.5 and 2.7 for the
84 values of the first two pK_a, respectively [23]. Recently, Ogden and coworkers found pK_{a2} and pK_{a3} values of 2.1 and
85 4.1 respectively in chloride media, while the pK_{a1} value could not be calculated [19].

86 Although these data are helpful for estimating the relative protonation of the resin and assessing the competition
87 between H^+ and Ni^{2+}, the counter-ion (here sulfate) also plays an important role. Not only must the pH buffering effect
88 near pH = $pKa_{HSO4/SO4}$ (=1.9) be significant, but the complexation effect must also be considered. In concentrated
89 solution, it forms complexes with Na^+ ($NaSO_4^-$), and with Ni^{2+}. Understanding the role of sulfate is therefore essential
90 for quantitative prediction of retention. In addition, its effects on sorption could be modified in the presence of other
91 metal cations known to react with it (*e.g.*, Ca^{2+}, Mg^{2+}).

92 Finally, whether protonated (H*bpa*$^+$ or H_2*bpa*$^{2+}$), or chelating a Ni^{2+} cation (Ni*bpa*$^{2+}$), resin groups carry a net
93 positive charge and are therefore anion exchangers. In sulfate media, the complexity is supplemented by the fact that
94 a "site-sharing" reaction occurs: a sulfate anion can be replaced by two bisulfate anions, resulting in the overall
95 adsorption of one molecule of sulfuric acid [24].

96 The objective of this work is to better understand the usefulness of Dowex M4195 resin in an acid solution derived
97 from dissolution of bio-ore ash to recover Ni. As this is a multicomponent solution, we focused on the sorption and
98 desorption steps with simpler model solutions. The main characteristics were kept, namely the presence of Na_2SO_4
99 at relatively high concentrations, the acid pH value (2) and the relevant Ni concentration, $c_{Ni} \approx 0.3$ mol/L. The influence
100 of Na_2SO_4 concentration was also investigated with the objective of better understanding its effect on pH and on the
101 retention of Ni and SO_4 by the resin.

The experimental results are interpreted using a model to describe the in-column transport coupled with reactions at thermodynamic equilibrium. This model will test the following hypotheses: retention is governed by the pH-dependent chelation of Ni by *bpa* groups and by the "site sharing" reaction that is suspected to play a key role in pH regulation. The model will allow us to calculate breakthrough curves during the adsorption and elution steps, and to fit constants by comparison with experimental curves. Finally, we will investigate whether the results obtained with the simplified solutions applies satisfactory to ash leachate solutions.

2. Materials and methods

2.1 Resin and solutions

Dowex M4195 resin (Sigma Aldrich, free form) is composed of a macroporous styrene-divinyl benzene matrix onto which bis-picolylamine functional groups (*bpa*) are grafted. It is available in the form of brown beads with a size of 0.3 to 0.8 mm, a moisture content of 40–60%, and a Cu capacity of 1.1 eq/L. Resin granulometry was verified by laser diffractometry using a Mastersizer 3000 (Malvern Panalytical). The measured median diameter (D_{50}) was 400 µm with a uniformity coefficient of 0.068.

Solutions were prepared using nickel sulfate hexahydrate (purity >99.5%, Sigma Aldrich), ACS reagent grade sulfuric acid (Sigma Aldrich), and sodium hydroxide pellets (purity >98.5%, Sigma Aldrich). Deionized water (Elga, Purelab Chorus) was used in all the experiments.

To prepare the pre-equilibration and loading solutions, sulfuric acid was diluted to the desired concentration, and the pH was then adjusted by additions of concentrated sodium hydroxide. Nickel sulfate was dissolved in the sodium sulfate solution and the pH was adjusted if needed. The final concentrations used for data treatment were the ones measured by ICP.

Nickel-rich leachates were obtained from hyperaccumulator plant ash (*Odontarrhena chalcidica*) as described in [9]. Aerial parts of *O. chalcidica* collected in Albania were ashed at 900 °C in a continuous biomass furnace (KWB Multifire MF2) with an average residence time of 20 min. Ash was sieved to 200 µm to remove unburnt particles. The ash was then washed twice using water to remove potassium (K), and then leached with sulfuric acid (2 mol/L) at

reflux for 2 h. After cooling and filtering, a Ni-rich solution was produced. The pH of the solution was increased to 2 using concentrated sodium hydroxide (Leachate 1) to permit Ni adsorption onto the resin. The same method was applied to a different batch of plant ash. This time, the solution produced was less acidic and H_2SO_4 was used to decrease its pH to 2 (Leachate 2) for comparison. The composition of the leachates is displayed in Table 1.

Table 1

Composition of the ash leachates adjusted to pH 2 with either NaOH or H_2SO_4.

	Leachate 1			Leachate 2		
	c (mol/L)					
Na	2.00	±	0.10	< 0.001		
S	1.68	±	0.08	1.09	±	0.05
Ni	0.24	±	0.01	0.37	±	0.02
Mg	0.28	±	0.01	0.48	±	0.02
K	0.18	±	0.01	0.26	±	0.01
P	0.030	±	0.002	0.167	±	0.008
Al	0.014	±	0.001	0.001	±	0.0001
Ca	0.008	±	0.001	0.016	±	0.001
Fe	0.003	±	0.0001	0.024	±	0.001
Mn	0.002	±	0.0001	0.001	±	0.0001
Zn	< 0.001			< 0.001		

The ash leachates are characterized by their high Ni content (up to 22 g_{Ni}/L) but contain large amounts of unwanted elements (mainly Mg, Fe, K).

2.2 Experimental set-up

The experimental set-up consisted of a volumetric pump (KNF), a borosilicate glass column (GE Healthcare, internal diameter 16 mm), an on-line conductivity detector, an on-line pH cell (Meterlab PH210) with a glass electrode

(Mettler Toledo), and a programmable fraction collector (Gilson). Conductivity and pH data were recorded with increments of 10 s. To pre-fill all the tubing, a by-pass circuit was arranged around the column.

The column was filled with resin beads suspended in deionized water and the height of the bed was adjusted by means of a piston, thus measuring 18 cm. The total bed volume was BV = 37 mL. The column was connected to the circuit and then the solutions were injected from the bottom upwards. For all experiments (except rinsing), the flow rate was set at 1 mL/min. The column itself was not thermo-regulated but experiments were conducted in a temperature-controlled room, with the temperature set to 20 °C.

2.3 Analyses

Elemental concentrations were determined by Inductively-coupled plasma emission spectroscopy (ICP-OES, Thermo ICAP 6000). External calibration was conducted using a certified solution (SCP-Sciences) in HNO_3 3 wt%. The calibration standards contained either Na, Ni, and S as analytes or a multi-element mix (Na, Ni, S, K, Ca, Mg, Fe, Mn, Zn, P, Cu, Co, Al, and Pb) depending on the sample composition. Prior to analysis, the experimental samples were diluted in the same matrix as the calibration standards (HNO_3 3 wt%). Solutions were analyzed in triplicate and the averaged values were retained. Concentration values with relative standard errors greater than 5% were rejected. Quality control checks using an independently prepared standard solution were performed every 12 samples to monitor drift and instrument accuracy.

2.4 Tracing experiments

The residence time distribution (RTD) of the fluid in the packed bed was measured by performing stepwise injections of tracing solutions at different concentrations. The column was pre-equilibrated with 0.15 mol/L Na_2SO_4 solution and fed with 1.02 mol/L Na_2SO_4 solution (positive steps) and *vice-versa* (negative steps). The conductivity of the outflow was used for the calculations. Measuring the RTD permitted to measure the porosity of the bed ε the porous volume Vp, defined as defined as $Vp = \varepsilon \times BV$. The number of mixing cells J was estimated conventionally with $J = (\bar{t}/\sigma)^2$, where $\bar{t}$ is the mean residence time, and σ the variance of the RTD.

2.5 Experimental protocols

Before the experiments, the resin bed endured five cycles of pre-equilibration, Ni loading, and elution. For all experiments, the resin bed was pre-equilibrated with the same Na_2SO_4 solution (pH 2) until the output conductivity and pH were identical to the input. It was then rapidly rinsed with deionized water at 10 mL/min for 8 min (2.2 bed volumes) and then fed with a Ni-rich solution (Table 2). After rinsing under the same conditions, elution was carried out with a concentrated sulfuric acid solution. The concentration of the eluting solution was 2 mol/L and decreased to 1.25 mol/L for the leachate 2 experiment in an attempt to save reagents.

During loading and elution, fractions were collected for analysis and weighted. The exact volume pumped was then calculated from the weights and densities of the fractions. The size of the fractions was chosen to have the best compromise between the representativeness of the effluent and an acceptable number of fractions. Small fractions (2 mL) were collected when the composition of outflow varied the most and larger fractions (up to 10 mL) when it varied the least. When it was known to be constant, intermediate samples were not analyzed.

Table 2.

Feed solutions for loading column experiments.

Feed solutions	c_{Ni} (mol/L)	$c_{\mathrm{SO_4}}$(mol/L)	c_{Na}(mol/L)	pH
Pre-equilibration	-	1.02	2.21	2
Sol. ref	0.31	0.95	1.15	2
Sol. -	0.31	0.60	0.64	2
Sol. +	0.30	1.12	1.85	2
Leachate 1	0.25	1.68	2.00	2
Leachate 2	0.37	1.09	-	2

3. Theory

3.1. Equilibrium model

A simple equilibrium model has been built to highlight the dominant mechanisms of the sorption process. To start-off, the dissociation and complexation reactions occurring in the solution are considered (Eqs (1)-(5)). They are assumed to follow a mass action law, with the corresponding stability constants (Table 3) extracted from the CHESS database at 25 °C and zero ionic strength [25]. No attempt was made to convert them to match the experimental conditions.

$$H_2O = H^+ + HO^- \quad (1)$$

$$H_2SO_{4(aq)} = H^+ + HSO_4^- \quad (2)$$

$$HSO_4^- = H^+ + SO_4^{2-} \quad (3)$$

$$Na^+ + SO_4^{2-} = NaSO_4^- \quad (4)$$

$$Ni^{2+} + SO_4^{2-} = NiSO_{4(aq)} \quad (5)$$

In the vicinity of the resin functional groups, nickel cations compete with protons for chelation (Eq. (6)). Here, the overbar represents the species in resin phase; Y stands for the counter anion, and *bpa* for the bis-picolylamine functional group.

$$\overline{H_2bpa,Y} + Ni^{2+} = \overline{Nibpa,Y} + 2H^+ \quad (6)$$

For the selected pH region, it was assumed that the functional groups were all doubly protonated. This is ensured by pre-equilibrating the resin with a concentrated Na_2SO_4 solution at pH 2. Indeed pH 2 is between the reported pK_{a1} and pK_{a2} of the resin [19,23]. Furthermore, the once protonated $bpaH^+,HSO_4^-$ form is a tautomer of $bpaH_2^{2+},SO_4^{2-}$ (Fig. 2). Thus, the first form can be treated equally as a doubly protonated form.

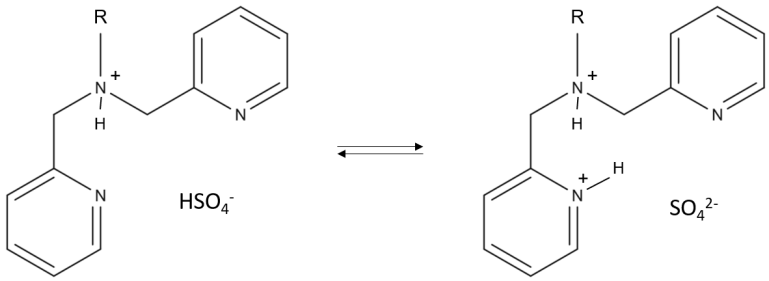

200

201

202 Fig. 2. Tautomerism of the protonated *bpa* group in a sulfate medium.

203 Assuming that the contribution of the sorbed counterion Y can be neglected, the reaction can be rewritten as Eq.

204 (7), which is similar to a classical cation exchange reaction.

205

$$2\overline{\mathrm{H}^{+}} + \mathrm{Ni}^{2+} = \overline{\mathrm{Ni}^{2+}} + 2\mathrm{H}^{+} \qquad (7)$$

206

207 Whether Ni is chelated or the resin protonated, anion exchange can occur as the functional group is positively

208 charged (Eq. (7)). In our conditions (pH 2), sorption of the HO- anion is practically inexistent. The sorption of the

209 $NaSO_4^-$ complex is assumed to be negligible in comparison to SO_4^{2-}: because of its net double charge, it should be

210 preferred for sorption [24]. For simplification, competition between HSO_4^- and $NaSO_4^-$ was neglected. Hence, anion

211 exchange reactions were reduced to the exchange of SO_4^{2-} with two HSO_4^- (Eq. (8)):

212

$$\overline{\mathrm{X}bpa,(\mathrm{SO_4})} + 2\mathrm{HSO_4^-} = \overline{\mathrm{X}bpa,(\mathrm{HSO_4})_2} + \mathrm{SO_4^{2-}} \qquad (8)$$

213

214 where X is indifferently 2H or Ni. This reaction can be rewritten as in Eq. (9) to better highlight its role as an acid

215 adsorption in the column.

216

$$\overline{\mathrm{X}bpa,(\mathrm{SO_4})} + \mathrm{H^+} + \mathrm{HSO_4^-} = \overline{\mathrm{X}bpa,(\mathrm{HSO_4})_2} \qquad (9)$$

217

This property is well-known for anion-exchanger with polyvalent functional groups in contact with polyacids and has been called “site-sharing” [24]. The selectivity constant K_9 is related to K_8 via Eq. (10).

$$K_9 = K_3 * K_8 \quad (10)$$

For simplification, Eq. (9) can be rewritten to yield Eq. (11), with the selectivity constant $K_{11} = K_9$. The ion exchange reactions considered are summarized in Fig. 3.

$$\overline{SO_4^{2-}} + H^+ + HSO_4^- = 2\overline{HSO_4^-} \quad (11)$$

To simulate the breakthrough curves of the ash leachates, the reactions described by Eqs (12)-(15) taking place in the aqueous phase were added. Sorption of the other anions and cations was not considered to limit the complexity of the model and the number of estimated parameters.

$$Ca^{2+} + SO_4^{2-} = CaSO_{4(aq)} \quad (12)$$

$$Mg^{2+} + SO_4^{2-} = MgSO_{4(aq)} \quad (13)$$

$$K^+ + SO_4^{2-} = KSO_4^- \quad (14)$$

$$H_3PO_{4(aq)} = H^+ + H_2PO_4^- \quad (15)$$

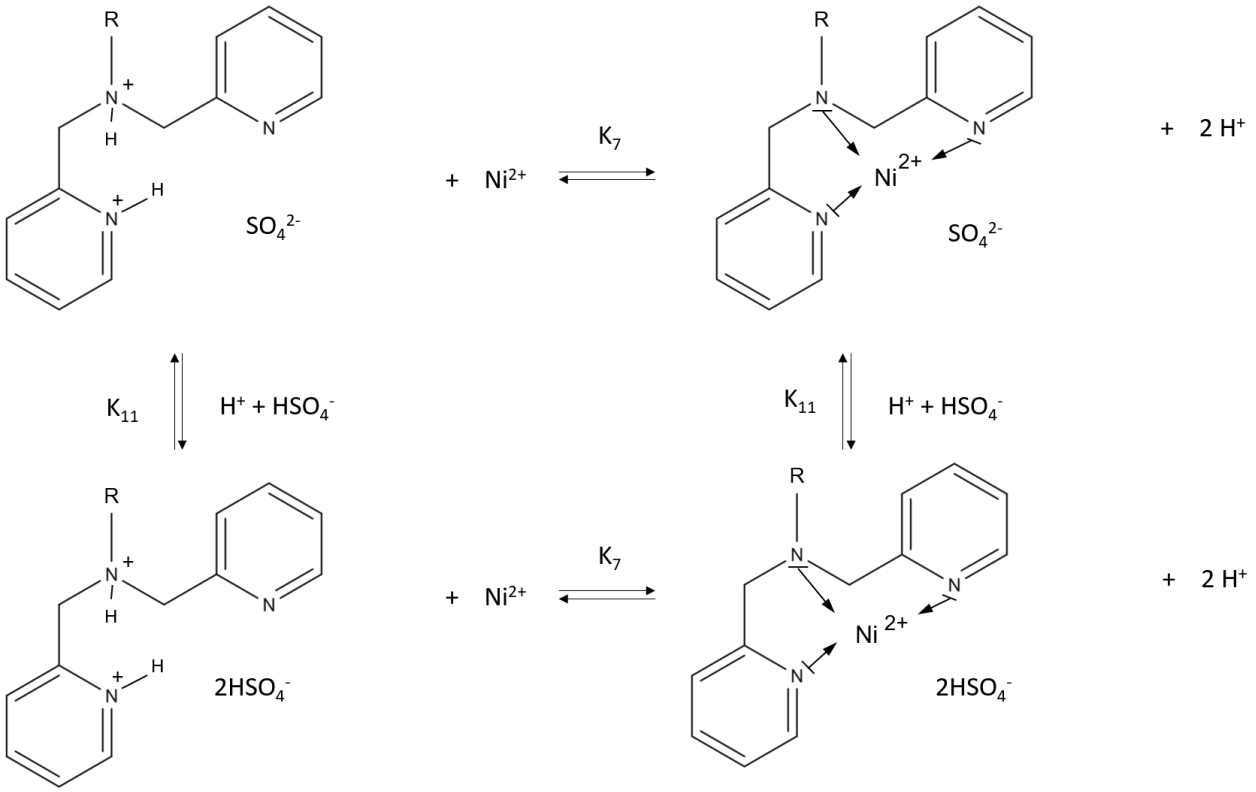

230

231 Fig. 3. Ion exchange reactions considered.

232 The cationic exchange capacity (CEC) and anionic exchange capacity (AEC) are defined by Eqs(16)-(17):

233

$$\mathrm{CEC} = n\left(\overline{\mathrm{H^+}}\right) + 2n\left(\overline{\mathrm{Ni^{2+}}}\right) \quad (16)$$

$$\mathrm{AEC} = n\left(\overline{\mathrm{HSO_4^-}}\right) + 2n\left(\overline{\mathrm{SO_4^{2-}}}\right) \quad (17)$$

234

235 where $n(A_i)$ is the quantity of fixed species A_i per unit of bed volume (in mol/L).

236 *3.2. Transport model*

237 Column hydrodynamics were modeled using the conventional model of mixing cells in series. Each cell is composed
238 of a stationary phase (resin) and a flowing phase (aqueous solution). To do so, the computer code IMPACT [26] was
239 used. As described in previous works [27–29], the code relies on the following assumptions:

240 - The cell geometry is constant, no shrinking or swelling of the resin is considered.

- Axial dispersion is accounted for in the number of mixing cells J, the Peclet number being equal to 2(J-1).
- Equilibrium is attained in each cell.
- The system is isothermal.
- Each phase is electrically neutral.
- No activity correction is performed.

Table 3.

List of the reactions implemented in the model.

Reactions in the aqueous phase	Equilibrium constant (25°C)	Reaction#
$H_2O = H^+ + HO^-$	$K_w = 10^{-14}$	(R1)
$H_2SO_{4(aq)} = H^+ + HSO_4^-$	$K_2 = 10^3$	(R2)
$HSO_4^- = H^+ + SO_4^{2-}$	$K_3 = 10^{-1.9}$	(R3)
$Na^+ + SO_4^{2-} = NaSO_4^-$	$K_4 = 10^{0.82}$	(R4)
$Ni^{2+} + SO_4^{2-} = NiSO_{4(aq)}$	$K_5 = 10^{2.13}$	(R5)
$2\overline{H^+} + Ni^{2+} = \overline{Ni^{2+}} + 2H^+$	K_7	(R7)
$\overline{SO_4^{2-}} + H^+ + HSO_4^- = 2\overline{HSO_4^-}$	K_{11}	(R11)
$Ca^{2+} + SO_4^{2-} = CaSO_{4(aq)}$	$K_{12} = 10^{2.11}$	(R12)
$Mg^{2+} + SO_4^{2-} = MgSO_{4(aq)}$	$K_{13} = 10^{2.41}$	(R13)
$K^+ + SO_4^{2-} = KSO_4^-$	$K_{14} = 10^{-0.88}$	(R14)
$H_3PO_{4(aq)} = H^+ + H_2PO_4^-$	$K_{15} = 10^{-2.16}$	(R15)

3.3. Calculations

Equilibria are calculated in each cell by minimizing the Gibbs enthalpy, using a Newton-Raphson algorithm. Inputs are the number of mixing cells J, composition of the pre-equilibrating feed solution, and the composition and injected volume of subsequent feed solutions. The washing and loading steps are successively modelled in the same simulation with the corresponding volumes.

The CEC and AEC are set by the user by defining the total amount of initially fixed species (Eqs(16)-(17)). The anionic capacity was set equal to the cationic one - determined experimentally - to maintain electroneutrality in the resin phase.

The program delivers the user the breakthrough curves for each defined species, expressed in mol/L, calculated as the outflow of the last mixing cell. Increments of 0.1 Vp were used for all the calculations. The concentrations of the different species were appropriately summed in a separate worksheet to allow comparison with experimental results (elemental concentrations) provided by ICP. The computed concentration of free H^+ in the column output (c_{H^+}) was converted to pH without activity correction (Eq. (18)).

$$\mathrm{pH} = -\log\left(c_{H^+}\right) \tag{18}$$

The elution curves for the two leachates were treated as follows: a hypothetical pool was calculated by summing only the fractions with $c_{Ni} > 0.1$ mol/L. The term "pool" or "pooled fractions" refers to the solution resulting from the addition of the considered fractions together. The value of 0.1 mol/L value was arbitrarily chosen to ensure that the purification of the eluates benefits from sufficiently high Ni concentration (*e.g.*, facilitating precipitation or electrowinning). The concentrations in the pool were conventionally calculated by integration of the elution curve between the chosen cuts. The integration step was defined by the fraction size of 2 mL, representing 0.1 Vp. The purity of the pooled solution was calculated as follows:

$$\mathrm{NiSO_4\ Purity} = \frac{c_{\mathrm{Ni},pooled}}{c_{\mathrm{Ni},pooled} + \sum_j c_{j,pooled}} \tag{19}$$

Where *j* belongs to {Na, Mg, Ca, K, PO_4, Zn, Mn, Fe}, and with all the concentrations in mol/L. Obviously, neither sulfate nor H^+ were considered as impurities because the medium is sulfuric acid. Solution purity was also calculated excluding Na to allow comparison between the two leachates.

4. Results and discussion

4.1 Determination of the model parameters

The residence time distribution (RTD) of the packed bed was determined from the results of the tracing experiments. Integration of the response curve revealed that the porosity ε of the bed was ε = 0.55, therefore the porous volume was Vp = 20.4 mL. The number of mixing cells in series was *J* = 56, which corresponds to a Peclet number of 110. The porous volume Vp was thus of 20.4 mL.

The resin bed capacity was determined by integrating the three breakthrough curves presented here (Figs 4 and 5). The Ni loading capacity was 0.53 ± 0.04 mol/L, or 1.06 ± 0.08 eq/L which is consistent with the manufacturer information concerning Cu [30]. Therefore, CEC = AEC = 1.06 ± 0.08 eq/L.

The breakthrough curves obtained when the column is fed with 1 Vp of water for rinsing, then fed solution Sol. Ref (Table 2) are displayed in Fig. 4 with calculated results in continuous lines. Firstly, the interstitial volume filled with pre-equilibrating solution is flushed. Then, the rinsing water breaks through, and from V/Vp = 1 the breakthrough curve of the feed solution Sol. Ref can be observed:

- at V/Vp = 2, the normality front appeared, corresponding to the sharp breakthrough of Na^+, not retained by the resin, accompanied by sulfate, the molar ratio Na/SO_4 being 2.0 ± 0.01 (on n = 6 data points).
- The second front started at V/Vp = 3.6, where Ni broke through sharply, consistently with a rapid pH decrease (down to pH 1). The nickel release rate was significantly slower after V/Vp = 4.4 as the pH of the effluent was stabilizing towards the nominal value of the feed solution. The release of Ni and H^+ was accompanied by that of sulfate.

These experimental breakthrough curves were used to determine the selectivity constants K_7 and K_{11}. These parameters were adjusted to fit the location of the Ni breakthrough and the shape of the sulfate concentration curve. The best fits were obtained by trial-and-error yielding K_7 = 0.05 and K_{11} = 0.0003. These values were kept for all subsequent simulations.

Despite the simplicity of the model and the many assumptions, the calculated breakthrough curves were in excellent agreement with the experimental ones. The first front, as well as the values of sulfate and sodium concentrations and pH on the plateau between 2 and 3.6 Vp were successfully predicted, as well as the shape of the front for Ni and total sulfate. The rise of pH to its nominal value was somewhat overestimated.

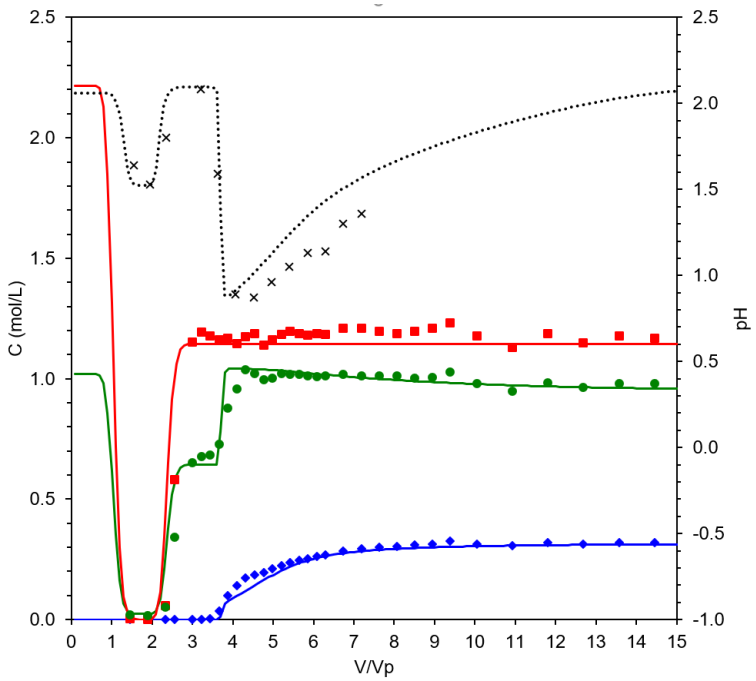

299

300 Fig. 4. Total nickel (blue diamonds), sulfate (green circles), and sodium (red squares) outlet concentration of the
301 resin bed while injecting the Sol. ref feed. pH values (crosses) are displayed with respect to the secondary axis.
302 Flowrate was of 1 mL/min (corresponding to 0.05 Vp/min) and the temperature was of 20 °C.

303 *4.2. Validation of the model with synthetic solutions*

304 4.2.1. Loading curves

305 The objective of the experiments with the Sol.+ and Sol.- feed solutions was to determine the influence of the
306 Na_2SO_4 background concentration. The breakthrough curves presented in figure 5 show that, in the considered
307 domain, this concentration did not affect Ni sorption. Indeed, the Ni breakthrough curves are practically identical in
308 the three cases. This later fact confirmed the reversibility of the sorption. Narrower pH variations were observed with
309 increasing Na_2SO_4 concentration, most likely related to the pH buffering capacity of the electrolyte.

310 The model performed equally for both Sol. + and Sol. – breakthrough curves, predicting fairly well the location of
311 the fronts and plateaus (Fig. 5). However, in both cases, the total sulfate concentration on the intermediate plateau
312 was underestimated by *ca.* 20%.

As observed experimentally, the predicted Ni front appears to be decomposable into a first slightly sharp front, followed by a broader one. Although this trend was not observed in practice, the predicted Ni profile was markedly sharper for the Sol. – feed (Fig. 5A) and broader for the Sol. + feed (Fig. 5B). In both cases, the pH rise for the second front is better predicted than in the previous case.

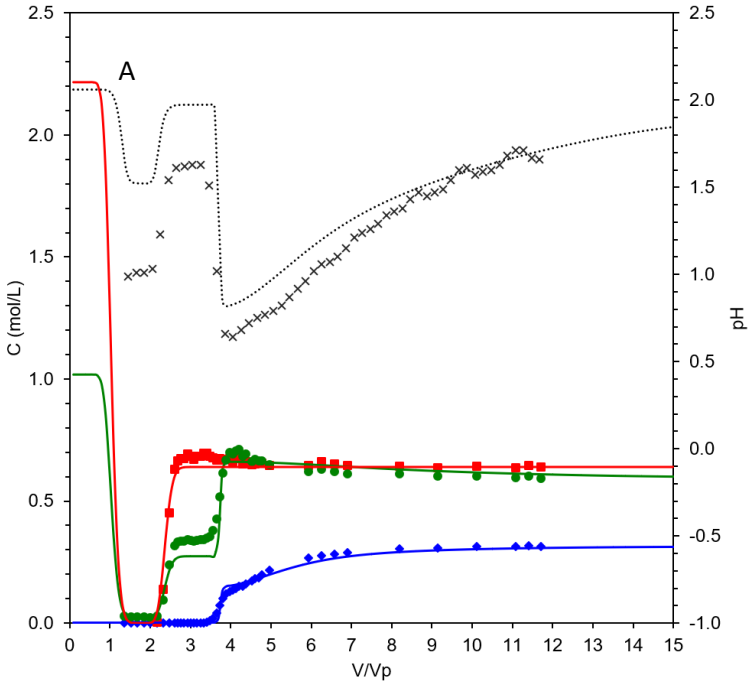

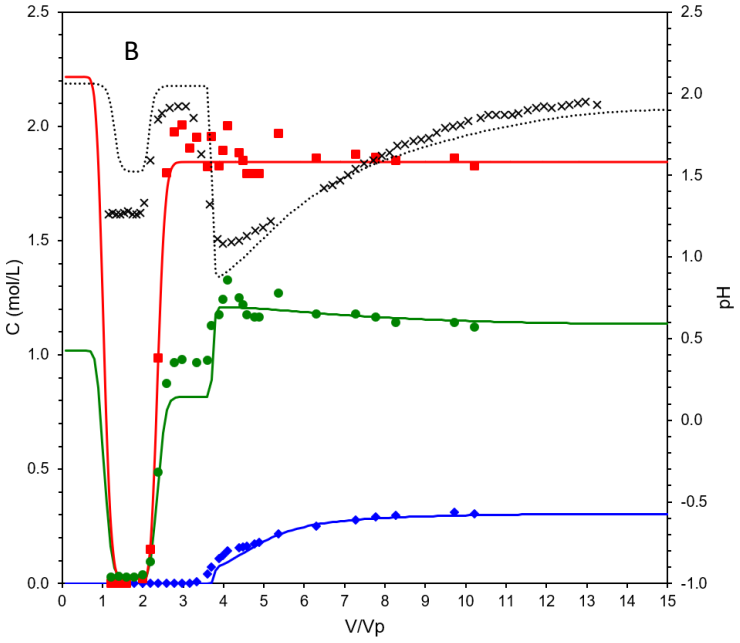

Fig. 5. Breakthrough curve for the feeds Sol. - (A) and Sol + (B). Total nickel (blue diamonds), sulfate (green circles), and sodium (red squares) outlet concentration of the resin bed. pH values (crosses) are displayed with respect to the secondary axis. Flowrate was of 1 mL/min (corresponding to 0.05 Vp/min) and the temperature was of 20 °C.

4.2.2. Elution curves

In all experiments, the elution performed with 2 mol/L H_2SO_4 permitted the recovery of all retained Ni. The elution after the loading with Sol. – is given as an illustration (Fig. 6). The model approximated the shape of the elution curves, yet, the experimental fronts were more diffuse than the calculated ones. Because the model has no activity correction implemented, the dissociation of the acids in presence (H_2SO_4 and HSO_4^-) was most likely overestimated, resulting in the overestimation of the free H+ concentration (negative pH). Therefore, Ni is displaced more sharply than experimentally observed. Another possibility is the third protonation of the resin, the latter taking up more protons than the model predicts.

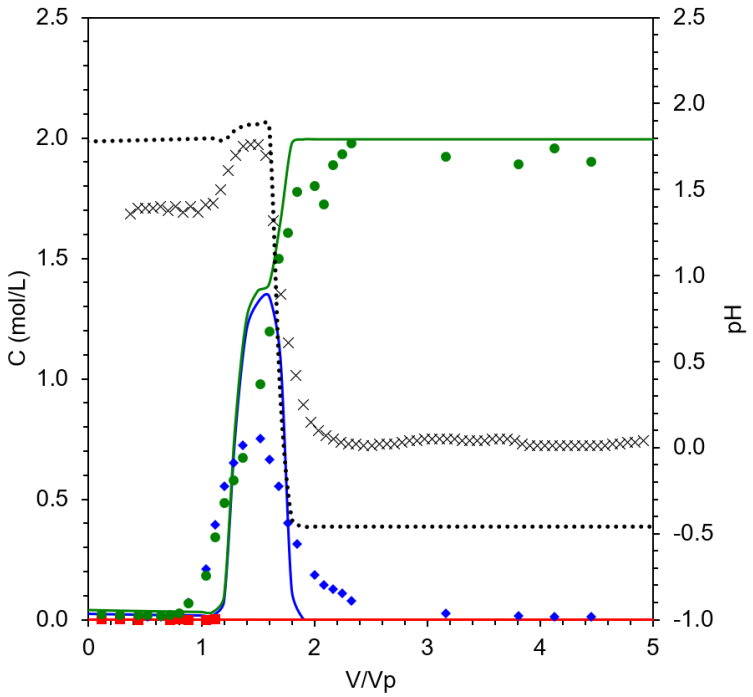

Fig. 6. Elution curve of resin bed with 2 mol/L H_2SO_4 after loading with the Sol. – feed. Total nickel (blue diamonds), sulfate (green circles), and sodium (red squares) outlet concentration of the resin bed. pH values (crosses) are displayed with respect to the secondary axis. Flowrate was of 1 mL/min (corresponding to 0.05 Vp/min) and the temperature was of 20 °C.

Even though the shape of the modeled elution curve differed from the experimental one, the amount of Ni eluted (calculated by integration) was rather consistent. The relative difference was of 5%, 12% and 12% for the elution after loading with Sol. –, Sol Ref, and Sol. +, respectively.

4.4. Application to multicomponent leachates

This work was undertaken in view of understanding and predict the loading and elution behavior of the resin bed with hyperaccumulator ash leachates with different characteristics, especially regarding their Na_2SO_4 concentration. The leachates also contained other cations (Mg, K, Fe) as well as notable amounts of phosphate (most likely in the form of phosphoric acid). Breakthrough and elution curves are presented Figs. 7 and 8.

Thanks to extremely favorable selectivity of the resin for Ni, and in the absence of Co and Cu, the other unwanted metals had little effect on Ni sorption. The breakthrough curves were highly similar to those obtained with the synthetic solutions, even when sodium was absent from the medium.

Interestingly, small amounts of Na were eluted during the loading of the resin with leachate 2 (Fig. 7B). This revealed that some $NaSO_4^-$ was bound to the resin during pre-equilibration, representing an uptake of 0.02 eq/L, but remained in minority (2% of the total capacity). It was easily replaced by HSO_4^- and/or SO_4^{2-}, thus confirming the assumption made in section 3.

In a first attempt, the complexation and dissociation reactions described by Eqs (12)-(15) were not implemented in the model and calculations resulted in poor fitting (not shown here). A good adequacy between calculated and experimental breakthrough curves was achieved after supplementing the model with the missing reactions (Fig. 7). The implementation was easy as stability constants were readily available. It quickly appeared that the pH buffering role of these reactions was determining at such a high ionic strength.

The calculated pH values varied much more than the experimental ones, and were underestimated during the Ni breakthrough ($\Delta pH \approx 0.2 – 0.4$). For both leachates, experimental Ni breakthrough was observed slightly earlier than predicted, with the same order of magnitude as for Feed Sol. + (Fig. 5B).

Similarly, to the experiments with synthetic solutions, retained Ni from the ash leachates was eluted by H_2SO_4. The elution curves are displayed in Fig. 8. Sodium in the eluate was searched for in the eluate fractions, but levels were extremely low. Lower acid concentration of the flushing solution resulted in peak broadening (Fig. 8B). Nonetheless, more than 96% of the fixed Ni was recovered by V/Vp = 4.

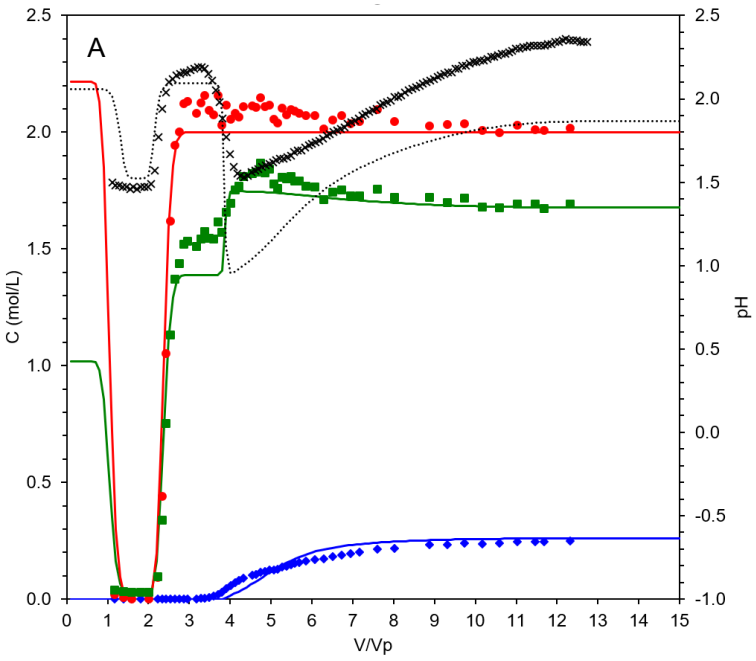

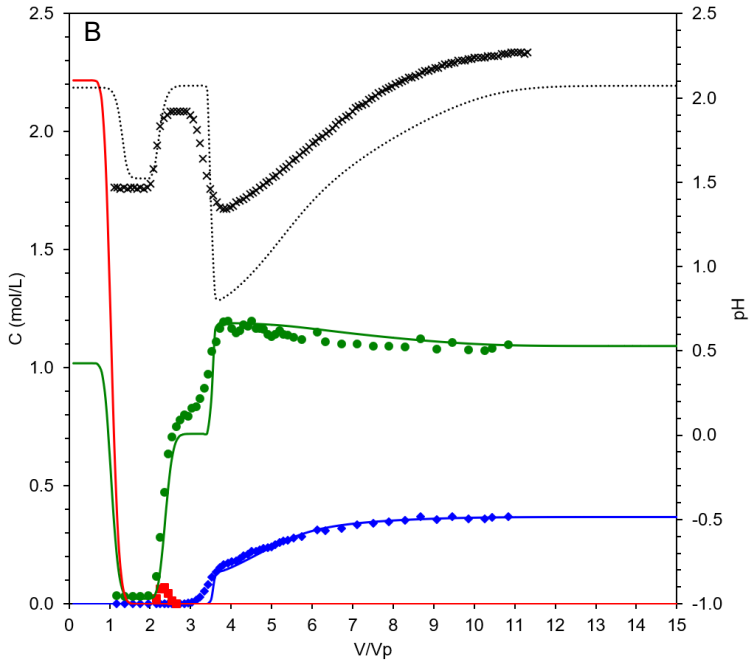

Fig. 7. Total nickel (blue diamonds), sulfate (green circles), and sodium (red squares) outlet concentration of the resin bed while injecting leachate 1 (A) and leachate 2 (B). pH values (crosses) are displayed with respect to the secondary axis. Flowrate was of 1 mL/min (corresponding to 0.05 Vp/min) and the temperature was of 20 °C.

Again, the model predicted correctly the location of the elution peak, the variation of the sulfate concentration and the pH variation. This time though, it failed to calculate precisely their shape, and the pH of the outflow was underestimated.

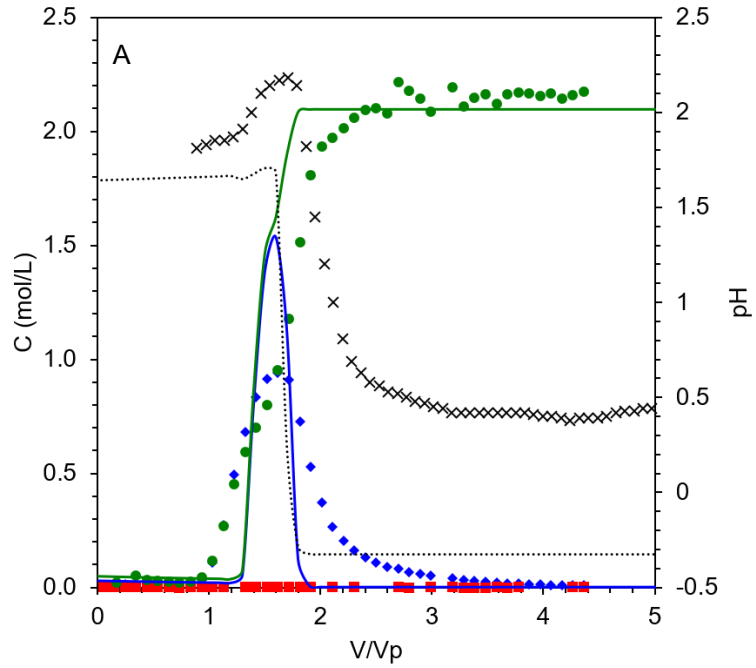

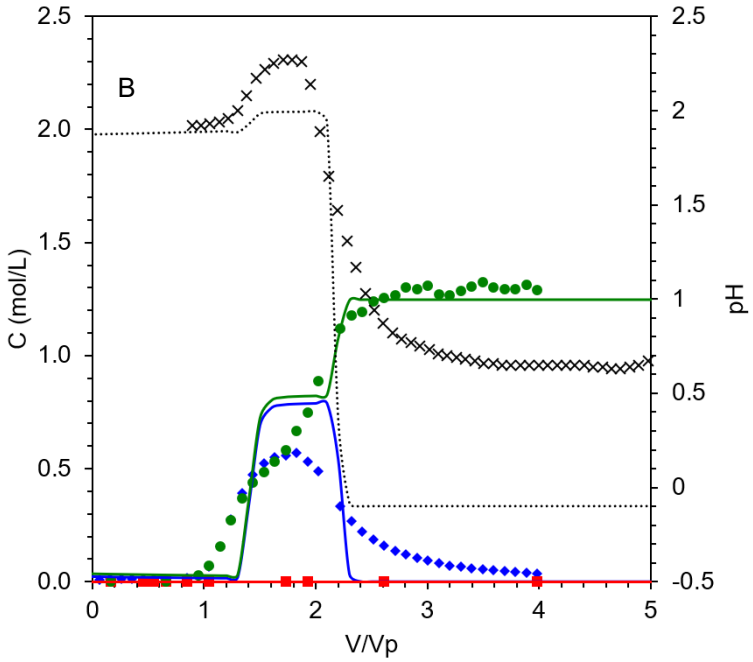

Fig. 8. Elution curves of the loaded resin with (A) Leachate 1, and (B) Leachate 2. Total nickel (blue diamonds), sulfate (green circles), and sodium (red squares) outlet concentration of the resin bed. pH values (crosses) are displayed with respect to the secondary axis. Flowrate was of 1 mL/min (corresponding to 0.05 Vp/min) and the temperature was of 20 °C.

4.5. Performance of the developed model

The model developed here using the IMPACT software confirmed that the dominating mechanisms were those that were already hypothesized. Quantitative prediction of the pH in the column is the primary driver, as pH is the main driver of Ni – H+ exchange. The implementation of the site-sharing reaction in the model resulted in an overall excellent prediction of the pH and Ni concentrations at the column outlet. The overall reaction scheme is based on a set of known reactions, whose constants are available, only two reactions and two parameters were added (selectivity constants K_7 and K_{11}). Moreover, this reaction scheme, even if it only includes reactions at equilibrium, allowed for a quantitative prediction of the number of elution fronts, their position and concentration variations. Finally, the calculated concentrations values were in excellent agreement with the experimental ones.

The approach proposed here is straightforward and easily reproducible: the equilibrium constants are input from readily available databases, then, specific selectivity constants are fit using a single reference experiment. Finally, the model can be applied to predict the loading behavior of a resin bed. The good fit also depends on the choice and number of assumptions (*e.g.*, protonation of the resin, isolation of the dominant mechanism involved, local equilibrium is reached at each step), that may not be valid in other experimental domains.

The model accuracy decreased when simulating the elution of the resin bed. This could be caused by several factors. Additional protonation of the resin was implemented using *bpa* dissociation reactions and the reported pK_{ai} values from the literature. However, no significant improvement was observed. The Donnan exclusion effect could have played a certain role in the loss of exactness. If the positive charge of the sorption sites (Ni*bpa*$^{2+}$) is not entirely masked by the counter anion (SO_4^{2-} or $2HSO_4^-$), the diffusivity of H+ in the pores could be limited. This would result in H+ not displacing chelated Ni not as sharply as the model predicts. In contrast, Ni approaches the sites in its neutral

complexed form ($NiSO_4$), it is therefore not subject to electrostatic repulsion. The most obvious reason for a decrease in model accuracy would stem from incorrect prediction of activity. When the sulfuric acid concentration increases up to 2 mol/L, dissociation of the acid (particularly bisulfate) appears to be overestimated, resulting in a negative pH and thus a sharp displacement of the chelated Ni by H^+. In forthcoming versions of the model, the implementation of activity coefficient models suited for high ionic strength will address this issue. Lastly, from a more practical aspect, it is conceivable that the online pH cell, situated after the column outflow, causes recirculation to the fluid, generating the tail of the Ni elution peak. Finally, assays are to be conducted to verify the effects of the flowrate. If required, the model could be modified to account for sorption kinetics, and/or mass transfer limitations (intra- and extra- particle diffusion).

4.6. Obtention of a $NiSO_4$ solution of high purity

Elution cuts defined by c_{Ni} > 0.1 mol/L (see section 3.3) represented a volume of 1.47 and 1.57 Vp for leachate 1 and 2 respectively. Their mean Ni concentration was 0.38 and 0.51 mol/L respectively (corresponding to 22 and 30 g_{Ni}/L). The purities of the leachates and of the hypothetically pooled solutions are presented in Table 4.

Table 4.

Purity characteristics of the leachates before and after purification with the conducted procedure

Solution	Leachate 1	Leachate 2	Leachate 1	Leachate 2
	Before purification		After purification	
$NiSO_4$ purity (%)	9 ± 1	29 ± 2	98.8 ± 0.3	96.9 ± 0.7
$NiSO_4$ purity (%)*	32 ± 2	29 ± 2	99.1 ± 0.2	96.9 ± 0.7
Impurity #1	Na	Mg	PO_4	PO_4
Impurity #2	Mg	K	Na	Ca

*: Excluding Na from impurities

Most of the impurities present in the leachate, namely Ca, Mg, K, Na, Fe, and Mn, were entirely removed during the rinsing step, prior to elution. The poor affinity of the resin for those elements can explain this result. Additionally, rinsing with DI water could have shifted the site-sharing equilibrium (Eq. 11), leading to the release of diluted H_2SO_4 [24], the latter eluting poorly-sorbed cations.

Phosphate is an important component of the leachate, and could rise issues if $Ni(OH)_2$ was to be precipitated directly from the leachates. Nickel phosphate ($Ni_3(PO_4)_2$) is quite insoluble (Ks = 4.74 10^{-32}) and should precipitate around pH 4-5, while $Ni(OH)_2$ precipitates in the pH 7-8 region [31]. As an illustration, raising the pH of the leachate 2 would result in the stoichiometric precipitation of 78% of the Ni as $Ni_3(PO_4)_2$.

With the conducted separation, phosphate concentration was reduced from 0.030 and 0.167 mol/L to 0.002 and 0.009 mol/L for leachate 1 and 2 respectively. The majority of the content has been removed, most likely displaced by the excess sulfate via ion-exchange during loading. A non-negligible fraction remains sorbed after the rinsing step, and is co-eluted with $NiSO_4$ becoming the first impurity in both eluates. Given the molar concentration in the purified solution, the resulting Ni losses through precipitation would however be minor (comprised between 1% and 4%, for leachate 1 and 2 respectively) and might be even further decreased. Phosphate removal could be conducted directly onto the loaded resin by circulating a concentrated Na_2SO_4 solution (at pH 2), the sulfate would displace the bound phosphate. Then, rinsing with water would remove lightly bound $NaSO_4^-$ and the interstitial solution. Finally, $NiSO_4$ could be recovered at purities higher than those displayed in Table 4.

In the scenario of recovering Ni through electrowinning, phosphate precipitation should not be an issue as it is typically conducted around pH 3.5 or lower in sulfate media [10,32]. Comparable Ni and PO_4 concentration levels (0.2 mol/L and 0.007 mol/L respectively) were met in the electrowinning experiment conducted by Lee [33] in which Ni is successfully recovered, although no information is given regarding the phosphate content of the produced cathode. In this case, the challenging impurity is likely to be Fe, even though its concentration in the purified solution does not exceed 5.10^{-4} mol/L. A sequential elution with dilute H_2SO_4, or with a scrubbing solution of $NiSO_4$, are conceivable answers to further improve purity.

The method permitted the isolation of Ni from the main leachates' impurities, and relatively high purities were obtained (≥ 97%). This was also possible because of the high affinity of the resin for Ni and the absence of metals with higher or comparable affinities (Cu, Co, U). The procedure paves the way for the production of a high value-added Ni, whether in the Ni hydroxide or ASNH salt form [9], or even cathodic Ni by electrowinning [10]. By avoiding the use of stoichiometric precipitants, cost savings were achieved regarding impurity removal, compared to published work. The

441 reusability of the resin is a key feature and should be monitored overtime. Our results, in consistency with other
442 previously published studies [15,16], suggest that a high number of sorption/desorption cycles can be performed
443 without capacity deterioration.

444 In the case of processing plant ash leachates, resin poisoning by metals that bind more strongly than Ni is unlikely.
445 Ni-specific hyperaccumulator plants (and their derived ash) contain trace amounts of Cu (generally on the order of
446 ppb). Contamination could only occur if important amounts of soil were retained with the treated biomass. It is
447 suggested that Cu contamination would result in a decrease in capacity, without affecting the purity of the produced
448 solution. Indeed, Cu elution on *bpa* resins has been reported to be almost impossible with sulfuric acid (up to 2 mol/L)
449 [20,34]. If detected, resin poisoning by Cu could be solved by eluting the resin bed with ammonia [34].

450 ## 5. Conclusions

451 One objective of this work was to better understand the functioning of the Dowex M4195 resin during the
452 adsorption/desorption of Ni in sulfate medium at pH 2 in the presence of Na_2SO_4. Column experiments with synthetic
453 solutions allowed to understand the dominant mechanisms involved: Ni competes with H+ for sorption on *bpa* groups,
454 while sulfate sorption on the resin plays a crucial role in pH regulation and significantly affects Ni sorption, by limiting
455 H+ activity. These hypotheses were tested by comparing experimental breakthrough curves with results calculated
456 using the IMPACT computational code, combining column transport and chemical reactions at thermodynamic
457 equilibrium. The reaction scheme with only two optimized constants, was found to be sufficiently accurate to
458 calculate the number and location of fronts, as well as concentration variations. Overall, a very good agreement was
459 obtained between the experimental and calculated values.

460 The use of this resin allowed the isolation of Ni sulfate from hyperaccumulator plant ash leachate to high purity
461 levels (up to 99%). The interest of this resin in the context of Ni valorization by the agromining chain of processes has
462 thus been confirmed. Compared to purification by precipitation, this technique has the advantage of saving expensive
463 reagents, in particular soda.

464

The approach proposed here aims at isolating the dominant sorption behavior, and secondarily consider the other elements. The complexity of the multi-metallic solution was reduced to a minimum, consisting of only the main metal (Ni), and the electrolyte (Na_2SO_4). Modelling the biphasic equilibrium, and especially pH, is crucial but can be easily conducted by equilibrium models as this work has highlighted. Then, the addition of the secondary elements (other cationic metals, but also anions such as phosphate) were subsequently considered. In this work, modelling their behavior properly in the solution, attained a good agreement between the calculated values and experimental values.

This work opens perspectives for the improvement of the process. Parameters critical for operation remain unexplored such as temperature and flowrates and need to be considered for higher throughput. Since feasibility has been proven and key mechanisms identified, more advanced process configuration has to be studied.

Declaration of competing interest

The authors declare that they have no competing financial interests or personal relationships that could have influenced the work reported in this paper.

Acknowledgements

This research was supported by Labex Resource 21 and European project Facce Surplus Agronickel No 652615. We gratefully acknowledge our colleague, Prof A. Bani (UAT, Tirana, Albania), for providing the HA plants. This work is included in the scientific program of the GISFI research consortium dedicated to the knowledge and the development of remediation technologies for degraded and polluted lands (Groupement d'Intérêt Scientifique sur les Friches Industrielles - http://www.gisfi.univ-lorraine.fr). The authors wish to thank the GISFI platform and technical staff for the burning of the plant biomass. They also warmly thank Dr. Antony van der Ent for the English editing.

References

[1] T.L.M. Exchange, LME Nickel | London Metal Exchange, Lme. (n.d.). https://www.lme.com/Metals/Non-ferrous/LME-Nickel (accessed January 23, 2022).

[2] R.L. Chaney, A.J.M. Baker, J.L. Morel, The Long Road to Developing Agromining/Phytomining, in: A. van der Ent, A.J.M. Baker, G. Echevarria, M.-O. Simonnot, J.L. Morel (Eds.), Agromining Farming Met., 2nd edition, Springer International Publishing, Cham, 2021: pp. 1–22. https://doi.org/10.1007/978-3-030-58904-2_1.

[3] R. Tisserand, A. van der Ent, P.N. Nkrumah, S. Sumail, G. Echevarria, Improving tropical nickel agromining crop systems: the effects of chemical and organic fertilisation on nickel yield, Plant Soil. 465 (2021) 83–95. https://doi.org/10.1007/s11104-020-04785-w.

[4] C. Hipfinger, M. Laux, M. Puschenreiter, Comparison of four nickel hyperaccumulator species in the temperate climate zone of Central Europe, J. Geochem. Explor. (2022) 106933. https://doi.org/10.1016/j.gexplo.2021.106933.

[5] D.M. Navarrete Gutiérrez, P.N. Nkrumah, A. van der Ent, J. Pollard, A.J.M. Baker, F. Navarrete Torralba, M.-N. Pons, J.A. Cuevas Sánchez, T. Gómez Hernández, G. Echevarria, The potential of *Blepharidium guatemalense* for nickel agromining in Mexico and Central America, Int. J. Phytoremediation. 23 (2021) 1157–1168. https://doi.org/10.1080/15226514.2021.1881039.

[6] A. Bani, G. Echevarria, S. Sulçe, J.L. Morel, Improving the Agronomy of *Alyssum murale* for Extensive Phytomining: A Five-Year Field Study, Int. J. Phytoremediation. 17 (2015) 117–127. https://doi.org/10.1080/15226514.2013.862204.

[7] P.N. Nkrumah, R.L. Chaney, J.L. Morel, Agronomy of 'Metal Crops' Used in Agromining, in: A. van der Ent, A.J.M. Baker, G. Echevarria, M.-O. Simonnot, J.L. Morel (Eds.), Agromining Farming Met., 2nd edition, Springer International Publishing, Cham, 2021: pp. 23–46. https://doi.org/10.1007/978-3-030-58904-2_2.

[8] B. Laubie, J. Vaughan, M.-O. Simonnot, Processing of Hyperaccumulator Plants to Nickel Products, in: A. van der Ent, A.J.M. Baker, G. Echevarria, M.-O. Simonnot, J.L. Morel (Eds.), Agromining Farming Met., 2nd edition, Springer International Publishing, Cham, 2021: pp. 47–61. https://doi.org/10.1007/978-3-030-58904-2_3.

[9] R. Barbaroux, E. Plasari, G. Mercier, M.O. Simonnot, J.L. Morel, J.F. Blais, A new process for nickel ammonium disulfate production from ash of the hyperaccumulating plant *Alyssum murale*, Sci. Total Environ. 423 (2012) 111–119. https://doi.org/10.1016/j.scitotenv.2012.01.063.

[10] R. Barbaroux, G. Mercier, J.F. Blais, J.L. Morel, M.O. Simonnot, A new method for obtaining nickel metal from the hyperaccumulator plant *Alyssum murale*, Sep. Purif. Technol. 83 (2011) 57–65. https://doi.org/10.1016/j.seppur.2011.09.009.

[11] X. Zhang, B. Laubie, V. Houzelot, E. Plasari, G. Echevarria, M.-O. Simonnot, Increasing purity of ammonium nickel sulfate hexahydrate and production sustainability in a nickel phytomining process, Chem. Eng. Res. Des. 106 (2016) 26–32. https://doi.org/10.1016/j.cherd.2015.12.009.

[12] D.B. Baskov, A.G. Bychkov, Process for extraction of nickel, cobalt and other metals from laterite ores, WO2015009204A2, 2015. https://patents.google.com/patent/WO2015009204A2/en (accessed January 12, 2022).

[13] L. Rosato, G.B. Harris, R.W. Stanley, Separation of nickel from cobalt in sulphate medium by ion exchange, Hydrometallurgy. 13 (1984) 33–44. https://doi.org/10.1016/0304-386X(84)90015-X.

[14] K.C. Sole, M.B. Mooiman, E. Hardwick, Ion Exchange in Hydrometallurgical Processing: An Overview and Selected Applications, Sep. Purif. Rev. 47 (2018) 159–178. https://doi.org/10.1080/15422119.2017.1354304.

[15] M.L. Strauss, L.A. Diaz, J. McNally, J. Klaehn, T.E. Lister, Separation of cobalt, nickel, and manganese in leach solutions of waste lithium-ion batteries using Dowex M4195 ion exchange resin, Hydrometallurgy. 206 (2021) 105757. https://doi.org/10.1016/j.hydromet.2021.105757.

[16] L. Ulloa, E. Bringas, M.-F. San-Román, Simultaneous separation of nickel and copper from sulfuric acid using chelating weak base resins, J. Chem. Technol. Biotechnol. 95 (2020) 1906–1914. https://doi.org/10.1002/jctb.6364.

[17] K. Sirola, M. Laatikainen, M. Lahtinen, E. Paatero, Removal of copper and nickel from concentrated ZnSO4 solutions with silica-supported chelating adsorbents, Sep. Purif. Technol. 64 (2008) 88–100. https://doi.org/10.1016/j.seppur.2008.08.001.

[18] J.K. Romary, J.D. Barger, J.E. Bunds, New multidentate α-pyridyl ligand. Coordination of bis(2-pyridylmethyl)amine with transition metal ions, Inorg. Chem. 7 (1968) 1142–1145. https://doi.org/10.1021/ic50064a018.

[19] M.D. Ogden, E.M. Moon, A. Wilson, S.E. Pepper, Application of chelating weak base resin Dowex M4195 to the recovery of uranium from mixed sulfate/chloride media, Chem. Eng. J. 317 (2017) 80–89. https://doi.org/10.1016/j.cej.2017.02.041.

[20] R.R. Grinstead, Selective absorption of copper, nickel, cobalt and other transition metal ions from sulfuric acid solutions with the chelating ion exchange resin XFS 4195, Hydrometallurgy. 12 (1984) 387–400. https://doi.org/10.1016/0304-386X(84)90009-4.

[21] J.T.M. Amphlett, S. Choi, S.A. Parry, E.M. Moon, C.A. Sharrad, M.D. Ogden, Insights on uranium uptake mechanisms by ion exchange resins with chelating functionalities: Chelation vs. anion exchange, Chem. Eng. J. 392 (2020) 123712. https://doi.org/10.1016/j.cej.2019.123712.

[22] A.K. Sengupta, Y. Zhu, Metals sorption by chelating polymers: A unique role of ionic strength, AIChE J. 38 (1992) 153–157. https://doi.org/10.1002/aic.690380116.

[23] C.V. Diniz, F.M. Doyle, V.S.T. Ciminelli, Effect of pH on the adsorption of selected heavy metal ions from concentrated chloride solutions by the chelating resin DOWEX M-4195, Sep. Sci. Technol. 37 (2002) 3169–3185. https://doi.org/10.1081/SS-120006155.

[24] F.G. Helfferich, Ion exchange, Dover ed, Dover Publications, New York, 1995.

[25] J. van der Lee, L. De Windt, CHESS Tutorial and Cookbook. Updated for version 3.0, Fontainebleau, France, 2002. http://chess.geosciences.mines-paristech.fr.

[26] M. Jauzein, C. Andre, R. Margrita, M. Sardin, D. Schweich, A flexible computer code for modelling transport in porous media: IMPACT, Geoderma. 44 (1989) 95–113. https://doi.org/10.1016/0016-7061(89)90021-9.

[27] M.-O. Simonnot, S. Ouvrard, Multicomponent anion exchange with a resin having weakly and strongly basic groups, Chem. Eng. Sci. 60 (2005) 1849–1858. https://doi.org/10.1016/j.ces.2004.11.027.

559 [28] N. Scholtus, E. Leclerc, P. De Donato, J.L. Morel, M.O. Simonnot, Eluto-frontal chromatography to simulate
560 chemical weathering of COx by low-molecular-weight organic compounds and early pedogenesis processes, Eur.
561 J. Soil Sci. 60 (2009) 71–83. https://doi.org/10.1111/j.1365-2389.2008.01088.x.
562 [29] K. Nsir, L. Svecova, M. Sardin, M.O. Simonnot, Transport of selenium oxyanions through TiO2porous media:
563 Column experiments and multi-scale modeling, J. Contam. Hydrol. 160 (2014) 30–41.
564 https://doi.org/10.1016/j.jconhyd.2014.02.004.
565 [30] Dow, Dowex TM M4195 Product Datasheet, n.d. https://www.lenntech.com/Data-sheets/Dowex-M-4195-L.pdf
566 (accessed January 5, 2022).
567 [31] J.R. Rumble, Solubility product constants, in: CRC Handbook of Chemistry and Physics, CRC Press, Boca Raton,
568 Fla., 2019.
569 [32] F.K. Crundwell, M.S. Moats, V. Ramachandran, T.G. Robinson, W.G. Davenport, Electrowinning of Nickel from
570 Purified Nickel Solutions, in: Extr. Metall. Nickel Cobalt Platin. Group Met., Elsevier, 2011: pp. 327–345.
571 https://doi.org/10.1016/B978-0-08-096809-4.10026-7.
572 [33] H.Y. Lee, Separation and Recovery of Nickel from Spent Electroless Nickel-Plating Solutions with
573 Hydrometallurgical Processes, Sep. Sci. Technol. 48 (2013) 1602–1608.
574 https://doi.org/10.1080/01496395.2012.756523.
575 [34] C.V. Diniz, V.S.T. Ciminelli, F.M. Doyle, The use of the chelating resin Dowex M-4195 in the adsorption of selected
576 heavy metal ions from manganese solutions, Hydrometallurgy. 78 (2005) 147–155.
577 https://doi.org/10.1016/j.hydromet.2004.12.007.